

Surface state influence on the surface lattice structure in Be(10 $\bar{1}0$)S.-J. Tang,^{1,2,*} H.-T. Jeng,^{3,1,†} Chen-Shiung Hsue,¹ Ismail,⁴ P. T. Sprunger,⁶ and E. W. Plummer^{4,5}¹Department of Physics and Astronomy, National Tsing Hua University, Hsinchu 30013, Taiwan²National Synchrotron Radiation Research Center, Hsinchu 30076, Taiwan³Institute of Physics, Academia Sinica, Nankang, Taipei 11529, Taiwan⁴Department of Physics and Astronomy, University of Tennessee, Knoxville, Tennessee 37996-1200, USA⁵Solid State Division, Oak Ridge National Laboratory, Oak Ridge, Tennessee 37831-6057, USA⁶Department of Physics and Astronomy, Louisiana State University, Baton Rouge, Louisiana 70806, USA

(Received 28 August 2007; revised manuscript received 21 November 2007; published 8 January 2008)

Three major surface related bands, S1, S2, and surface resonance, of Be(10 $\bar{1}0$) dispersing in the large projected bulk band gaps from \bar{A} to $\bar{\Gamma}$ are reexamined by first-principles calculations. A comparison between experimentally and theoretically determined surface electronic structure reveals that charge redistribution dictates and explains the observed abnormal inward relaxation ($T=0$) and thermal contraction ($T>0$) of the surface lattice structure. Through first-principles calculations, possible mechanisms of this synergistic interplay between the electronic and lattice structures are proposed.

DOI: 10.1103/PhysRevB.77.045405

PACS number(s): 73.20.At, 71.15.-m, 79.60.-i, 68.35.B-

I. INTRODUCTION

Breaking the translational symmetry of a lattice by the creation of a surface will create redistribution in charge and will change the structure near the surface. The interplay between the charge and the structure has been a fundamental issue in the field of surface science. Smoluchowski¹ explained the surface dependence of the work function by the charge redistribution parallel to the surface, and Finnis and Heine² used this concept to explain the crystal face dependence of the change in interplanar spacing. Landman *et al.*³ extended this electrostatic model and found that there is, in general, a simple correlation between the stacking sequences of the crystal and the oscillatory relaxation. Feibelman⁴ also pointed out that the electronic configuration of an atom at the surface affected the interplanar spacing. On the other hand, a surface itself is a defect to the bulk so there will be Friedel oscillations creating a charge modulation of wave vector $2k_F$, which can drive a lattice distortion perpendicular to the surface. Cho *et al.*⁵ showed that for simple metals such as Al, Mg, and Be, Friedel oscillations in the charge density caused by the redistribution of the electrons to screen the presence of the surface drove an oscillatory interplanar relaxation. Another obvious source of a new electronic charge distribution at the surface is surface states in the projected bulk band gaps. There has been a speculation about the importance of surface states on the physical and chemical properties of a surface,⁶ but the evidence is not definitive. Chis and Hellising, through a theoretical investigation of the relaxation of the simple metal surface Al(100), found that the degree of surface relaxation convergence, with respect to the number of slab layers, is determined by the location of the surface state band relative to bulk bands,⁷ and Lee *et al.*⁸ concluded that taking into account surface relaxation only slightly improves the overall agreement between the binding energies of features of the calculated surface electronic structure of Al(110) and the experimental data.

Beryllium is an ideal system to elucidate the influence of surface states on the surface lattice structures. Because of the

large surface to bulk ratio of density of states at E_F , the surface state in Be(0001) has been considered as one of the best model to investigate the purely two-dimensional (2D) electronic system. In addition to a large surface core level shift and giant surface Friedel oscillations in this surface,^{9,10} there is a strong electron-phonon coupling of the surface state in Be(0001), which, as determined by angle-resolved photoemission measurements,^{11–13} has been found to have the $\lambda \sim 0.7$, three times larger than the bulk value. Another more open surface of beryllium, Be(10 $\bar{1}0$), also possesses very localized surface electronic structures, which, however, are considered to be more covalentlike even though they have a similar qualitative behavior as that described above for Be(0001).^{14,15} Hofmann *et al.*¹⁶ proposed a model of directional back bonding to explain the measured large inward relaxation of $\sim 25\%$ between the first layer and the second layer on Be(10 $\bar{1}0$). Furthermore, Cho *et al.*¹⁷ attributed the observed surface core level shifts, which persist down to the fifth layer in Be(10 $\bar{1}0$), to the stiffness of electrons that are not able to screen the influence of the surface. Ismail *et al.*¹⁸ carried out a temperature-dependent low energy electron diffraction (LEED)-IV measurement of the Be(10 $\bar{1}0$) surface and showed that the top four layers of Be(10 $\bar{1}0$) thermally expand in a damped oscillatory way. From this LEED-IV result, the interlayer spacing, d_{12} , between the first layer and the second layer has been shown to contract further with increasing temperature, namely, $\Delta d_{12} = -23.5\%$, -26.7% , and -30.8% at the temperature of 110, 300, and 500 K, respectively, where $\Delta d_{12}(T) = [d_{12}(T) - d_{12}^{bulk}(T)] / d_{12}^{bulk}(T)$. The thermal data are in good agreement with calculations within the quasiharmonic calculations.¹⁹ At the present, no definitive correlation has been found between the role of surface states and the $T=0$ K large inward relaxation or the finite temperature thermal contraction of the surface layer. However, in an earlier paper, Tang *et al.*²⁰ found that the energy of the most localized surface state S1, which disperses in the middle of the large bulk-projected band gap at \bar{A} , shifts with increasing

temperature in the direction opposite to that for a bulk state. Based on this observation, the interplay between the S1 surface state and the thermal contraction of the first layer on Be(10 $\bar{1}0$) was speculated. Theoretical calculations of surface electronic bands in Be(10 $\bar{1}0$) were implemented previously;^{21–23} However, focus was only on the comparisons of the energy positions between the calculated surface state bands of $T=0$ relaxed surface and the corresponding measured results. *The influence of the surface states on the surface structures or vice versa was overlooked.* In this paper, we have performed first-principles calculations to obtain the surface state band dispersions between \bar{A} and $\bar{\Gamma}$ by adopting structural experimental data from the previous temperature-dependent LEED-IV study.¹⁸ By employing these experimentally determined interlayer spacings of the top four layers, d_{12} , d_{23} , d_{34} , and d_{45} , at different temperatures, the resulting calculated surface state bands were carefully compared with those measured by photoemission. The degree of consistency between the former and the latter would definitely reflect the relationship between the surface states and surface structures.

II. THEORETICAL AND EXPERIMENTAL DETAILS

The band structure calculations were performed using the full-potential projected augmented wave method²⁴ as implemented in the VASP package²⁵ within the local density approximation. The Be(10 $\bar{1}0$) surface was simulated using a 24-layer Be slab (thickness of ~ 22 Å) with a vacuum thickness of ~ 10 Å, separating the slabs well. The self-consistent calculations were performed on a 48 k points mesh over the irreducible two-dimensional Brillouin zone using 17 640 plane waves with a cutoff energy of 248 eV. Calculation began with a determination of the surface band structure with both the long-layer and short-layer terminations truncated from bulk lattice along the (10 $\bar{1}0$) direction. The ground state structures of both terminations were then optimized to yield $T=0$ atomic plane positions. It was found that the theoretically obtained interlayer spacing of $\Delta d_{12,theory} = -21.58\%$, $\Delta d_{23,theory} = 5.41\%$, $\Delta d_{34,theory} = -11.52\%$, and $\Delta d_{45,theory} = 3.87\%$ for the short-layer terminated case compared very well with those of the low temperature LEED-IV study,¹⁸ which found very similar results for $d_{12,exp} \sim -22\%$, $\Delta d_{23,exp} \sim 5\%$, $\Delta d_{34,exp} \sim -14\%$, and $\Delta d_{45,exp} \sim 2\%$. Based on the obtained optimized short-layer surface structure, the temperature-dependent band dispersions were then calculated by taking into account the temperature induced change in interlayer spacing observed by Ismail *et al.*¹⁸ Finally, the calculated results were compared with the measured data, as discussed below.

The photoemission experiments were performed at the Advanced Light Source (ALS) on Beamline 10.0.1 using a high-resolution Scienta 2002 energy analyzer at 40 eV photon energy with total energy resolution of 10 meV and angular resolution of $\pm 0.15^\circ$ in 6×10^{-11} Torr vacuum and at $T = 30$ K. The cleaning procedure for the Be(10 $\bar{1}0$) sample was described earlier.²⁰ The clean Be(10 $\bar{1}0$) sample produced a sharp (1×1) LEED pattern.

III. RESULTS AND DISCUSSION

Figures 1(a) and 1(b) show the calculated surface state bands of S1, S2, and surface resonance (SR) dispersing from \bar{A} and $\bar{\Gamma}$ for the long-layer termination and short-layer termination of the Be(10 $\bar{1}0$) relaxed surface, respectively. Due to the interactions of two surfaces of the slab model, each surface state has two bands for different symmetries.⁶ The red curves in Fig. 1 represent the discrete bulk bands derived from the finite thickness of the slab model. In addition to differences between the energy positions of the three surface state bands between the two different terminations, one can easily see that the band dispersions of both the S2 surface state and the SR surface resonance for the short-layer termination are not free-electron-like; that is, the minimum of the S2 band and the maximum of the SR band are located at $0.2\text{--}0.4$ Å⁻¹ away from the zone-boundary point \bar{A} . Figure 1(c) shows an experimental 2D photoemission image of measured surface state bands with the measured data adopted from Ref. 20, indicated by green squares, and the calculated short-termination results of Fig. 1(b) superimposed. As is shown, not only the energy positions but also the non-free-electron band shapes of the experimentally measured S2 and SR bands are consistent with calculated results. This strong agreement between theory and experiment strongly supports a Be(10 $\bar{1}0$) surface short-layer termination model. It also appears that this preference for short-layer termination has to do with the non-free-electron behaviors of the surface states on Be(10 $\bar{1}0$). It is not unusual that the S2 surface state and SR resonance hybridize with each other. S2 has a p_y symmetry, and SR has s and p_z symmetries.²¹ A plausible explanation for the contraction of the Be(10 $\bar{1}0$) surface has been proposed by Feibelman.²⁶ Namely, as the outer layer moves inward, the bonding to the second-layer atoms becomes not only shorter, but also significantly closer to the surface plane. This makes it advantageous to move p_z electrons into p_x and p_y orbitals. Furthermore, hybridizations of the S2 and SR states is a direct reflection of this explanation and is also consistent with Hoffman's model of directional back bonding to explain the large inward relaxation of 25% between the first layer and the second layer observed on Be(10 $\bar{1}0$).¹⁶ Figure 1(d) shows the S1, S2, and SR bands of the same symmetry for both relaxed and truncated surfaces. As is seen, upon relaxation, there is an evident change for the S2 band in the portion from \bar{A} to the minimum of the band, and for the SR band in the portions from $\bar{\Gamma}$ to the maximum of the band. Our calculation shows that these portions of S2 and SR bands contribute more densities of states in the surface region, which also correspond to the intense part of photoemission data in Fig. 1(c). Figures 2(a) and 2(c) show the contours of the charge density distributions near the surface layer (~ 22 Å) for S2 at the k_{\parallel} position corresponding to the minimum of the band and for SR at the k_{\parallel} position corresponding to the maximum of the band, respectively, in the (0010) cut plane. The S2 band, with a σ bond character, connects adjacent atoms of the surface layer in the (0001) direction; furthermore, in the (10 $\bar{1}0$) direction, there is large

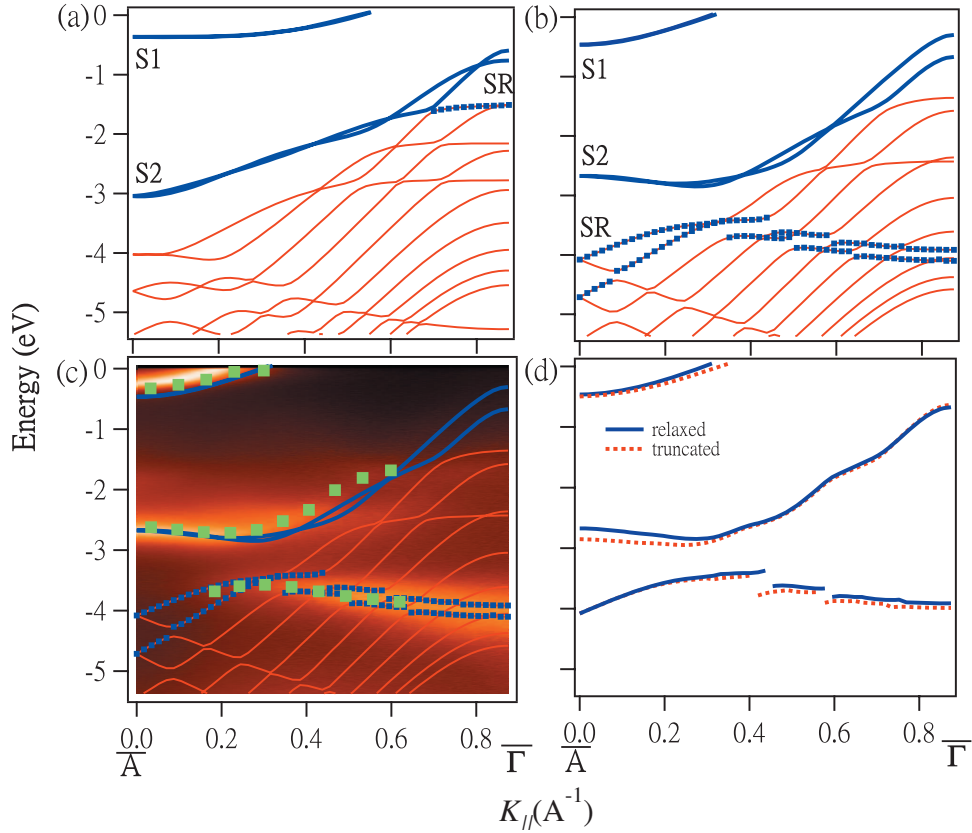


FIG. 1. (Color) The surface state band dispersions of S1 and S2 surface states (blue curves) and SR surface resonance (blue dots) dispersing from \bar{A} and $\bar{\Gamma}$ (k_{\parallel} with respect to \bar{A}) of the Be(10 $\bar{1}0$) relaxed surface for (a) long-layer termination (calculation), (b) short-layer termination (calculation), and (c) short-layer termination (calculation and measurements). Green squares are the measured data adopted from Ref. 20. (d) The calculated S1, S2, and SR band dispersions of the same symmetry for relaxed and truncated surfaces.

charge overlap within the region between the first and second layer, and that between the second and fourth layers. In the same way, the SR band, with a π bond character, connects the adjacent atoms of the surface layer in the (0001) direction, and in the (10 $\bar{1}0$) direction, there is also a large charge overlap within the region between the first and second layers and that between the second and fourth layers. Comparing Fig. 2(a) with 2(c), one can observe that the bonding structures of the S2 in the region between the first and the fourth layer resemble those of the SR as a result of the proposed hybridization, which determines the bonding between the atoms of adjacent layers in the (10 $\bar{1}0$) direction. The charge density distribution contours on the same plane are then integrated to form z profile expressions for the relaxed and bulk truncated surface, as shown in Figs. 2(b) and 2(d). Upon surface relaxation, there is no relevant change of charge density in the region between the first layer and the fourth layer for the S2 band; however, for the SR band, there is a large increase in the charge density in this region. Having p_z and s symmetries, the SR band has 50% of the charge from the dangling bonds above the top layer.²¹ Through this hybridization of the S2 and SR bands, the charge densities of SR effectively accumulate in the regions near surface atoms, attracting the positive ion cores toward the bulk of the crystal. This is again confirmed in Fig. 2(d), where the peak near the first layer increases largely when the surface relaxes and the

layer spacing between the first and second layers, in turn, contracts, as indicated by the arrows.

Relaxation is the change of interlayer spacing in the surface layers with respect to the corresponding bulk values at $T=0$. When the temperature increases from zero, the interlayer spacing of the surface layers then thermally contracts or expands. According to the LEED-IV measurement of Ismail *et al.*,¹⁸ the first short-layer interspacing contracts even further with increasing temperature. One important observation to note is that the degree of the contraction with increasing temperature (e.g., 7.8% from 110 to 500 K) is much less than the $\sim 25\%$ contraction due to the relaxation ($T \cong 0$) from the bulk truncated surface. Moreover, this may imply that the temperature-dependent contraction is driven by a different mechanism. Thermal expansion (or contraction) of the surface layer can be determined from the surface free energy $F(d_{12}, T)$ in the quasiharmonic approximation,^{19,27}

$$F(d_{12}, T) = E_{stat}(d_{12}) + \sum_i F_{vib}^i(d_{12}, T). \quad (1)$$

The first term is the static interlayer potential. The second term is the vibrational energy and entropy. As for the thermal expansion, both terms (static and vibrational) are equally important in the sense that when the temperature increases, the surface charge rearranges and, in turn, the vibrational prop-

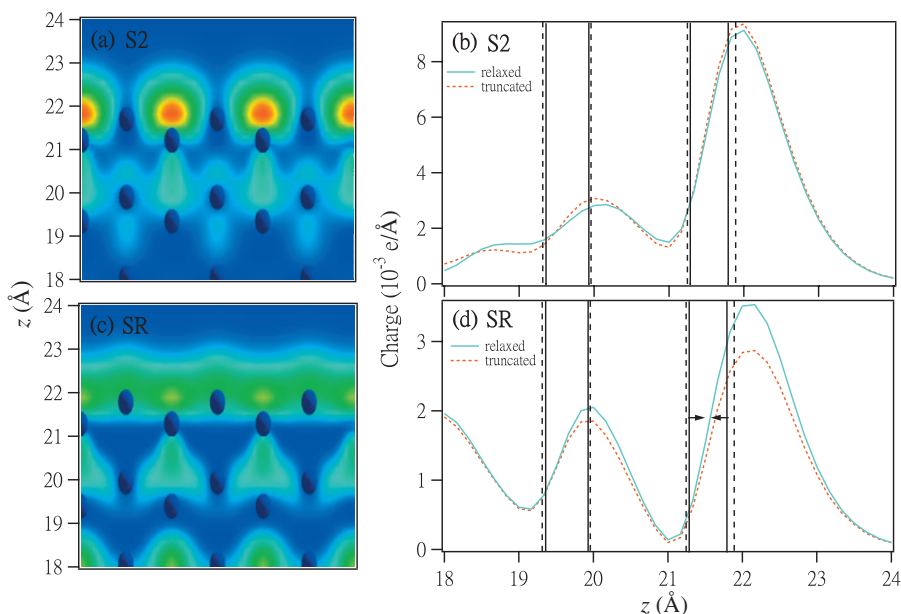


FIG. 2. (Color) (a) The charge density distribution contours corresponding to the k point at the minimum of the S2 surface state band in the (0010) cut plane for the relaxed surface at $T=0$ K. (b) The charge density z profile for the S2 surface state. The solid and dashed bars correspond to the positions (from the right to the left) of first, second, third, and fourth layers for the relaxed and bulk truncated surfaces, respectively. (c) The charge density distribution contours corresponding to the k point at the maximum of the SR resonance state band in the (0010) cut plane for the relaxed surface at $T=0$ K. (d) The charge density z profile of the SR resonance state. The solid and dashed bars correspond to the positions (from the right to the left) of first, second, third, fourth layers for the relaxed and bulk truncated surfaces, respectively.

erties of the atoms in all the directions would change such as to minimize the surface free energy.^{19,27}

In the present case, the S1 surface state with p_z and s symmetries has up to 70% of the charge distributed above the top surface layer.²³ The strong localization of the S1 surface state makes it the best candidate for the study of the interplay between the thermal contraction of the surface layer and the surface state. Figure 3 shows the temperature dependence of the energy shift for S1 and S2 surface states at \bar{A} . The hollow square and solid square symbols refer to the measured results from Ref. 20, and the hollow triangle and solid triangle symbols correspond to the present first-principles calculated results. In spite of an energy offset, due in part to the surface quality of the sample²⁸ and also the theoretical limitations,²² both measured and calculated results show a consistent trend that with increasing temperature, the S2 surface state shifts toward the Fermi level but the S1 surface state shifts away from the Fermi level. The binding energy of the S2 surface state is just 1.5 eV above the bulk band edge at \bar{A} , and it has at least 40% charge distributed more deeply than the first two layers.²³ Therefore, its temperature-dependent behavior must be closely tied to the bulk states, just as in the case of the Shockley surface states of noble metal surfaces, which have long decay lengths into deeper layers.²⁹ As opposed to the S2 surface state, the temperature dependence of the S1 surface state is presumed to be closely related to the lattice behavior of the surface layer. With respect to the change in binding energy with temperature, it is worth noting that a much better agreement between the measurement and calculation is found for the S1 state rather than for the S2 state. Specifically, the close agreement

between the theoretical and experimental values of the temperature-dependent slope of energy, as shown in Fig. 3, is due to the fact that only the temperature-dependent interlayer spacings for the top four layers, which accommodate all the S1 charge densities, are used in the calculation. Figure 4(a) shows the charge distribution contours of the S1 surface state at \bar{A} . In addition to the large charge density (70%) located on top of the first layer, one can see that the remaining S1

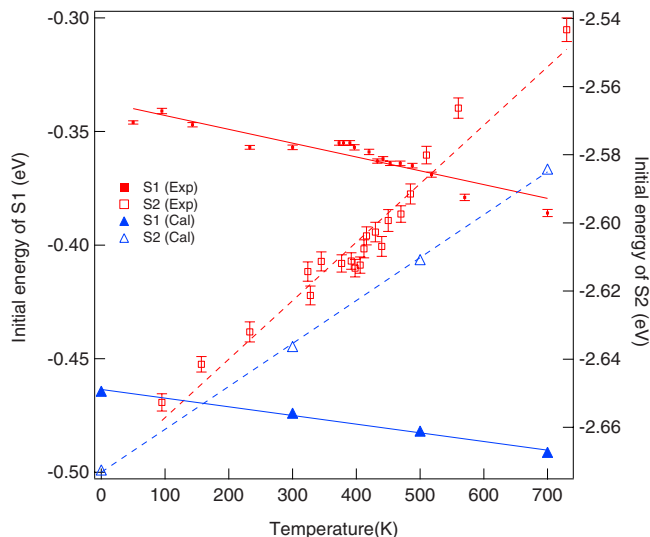


FIG. 3. (Color online) The temperature-dependent energy shifts for S1 and S2 surface states: measurement (square marks) and calculations (triangle marks). The solid (dashed) lines are for linear fits of S1 (S2).

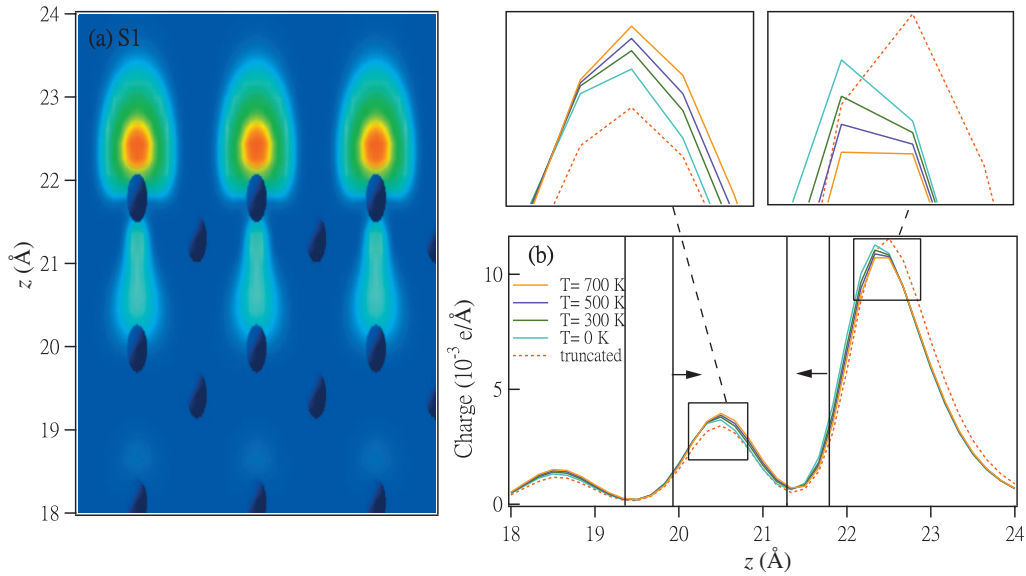


FIG. 4. (Color) (a) The charge density distribution contours of the S1 surface state at \bar{A} in the (0010) cut plane for the relaxed surface at $T=0$ K. (b) The charge density z profile of the S1 surface state for the bulk truncated surface and the relaxed surface at $T=0, 300, 500,$ and 700 K. The solid bars correspond to the positions (from the right to the left) first, second, third, and fourth of layers for the relaxed surface at $T=0$.

charge density is predominately distributed between the first and the third layer, causing the attracting force between them. Figure 4(b) shows the corresponding z profiles of the charge density distribution of the S1 surface state for bulk truncated and relaxed surfaces corresponding to temperatures of 0, 300, 500, and 700 K. When the surface relaxes at $T=0$ K, one can see from the z profile of the charge density that the peak above the first layer shifts toward deeper layers. In short, this is the so-called Smoluchowski effect^{1,26} in which the charge density corrugation minimizes in order to reduce the electron kinetic energy. In addition to the hybridization of the S2 and SR discussed in the previous section, the Smoluchowski effect on S1 also certainly contributes to the large inward relaxation of the Be(10 $\bar{1}$ 0) surface. Furthermore, when the temperatures increases from 0 to 700 K, one can see that the peak of the charge density above the top layer remains stationary but gradually attenuates, as clearly shown in the right inset of Fig. 4(b). On the other hand, the peak of the charge density between the first and the third layer continues to increase, as shown in the left inset of Fig. 4(b).³⁰ Charge accumulation between the first and third layers affects both the static and vibrational parts of surface free energy. As for the static part, increased charge density of states between the first and the third layer would shift the minimum of the static interlayer potential to shorter spacing, which, in turn, would increase the propensity for the surface layer to move further inward with increasing temperature, as indicated by the arrows in Fig. 4(b). As for the vibrational part, according to the NN bond length picture developed by Narasimhan³¹ for the thermal contraction of fcc(110) surfaces, there is a large enhancement in the coupling between the first and the third layer of the relaxed surface, which strongly reduces the amplitudes of the out-of-planes vibrations of atoms in the first layer. Because of similar geometric arguments, first- and third-layer couplings are also expected

for the Be(10 $\bar{1}$ 0) surface. Moreover, rather than effects due to an anharmonic interlayer potential, the observed thermal contraction of this system was attributed to a reduction in the first-layer vibrational amplitude perpendicular to the surface with respect to the one parallel to the surface.^{18,19} It is without any doubt that the increase of S1 charge density between the first and the third layer with increasing temperature further facilitates an increase in the force constant and hence reduces the first-layer vibrational amplitude perpendicular to the surface. Lazzeri and de Gironcoli,¹⁹ by using the first-principles calculation within the quasiharmonic approximation, found that the large density of states of the lowest phonon branch is spatially located on the second surface layer instead of the first layer. This is in line with the result found by Tang *et al.*,²⁰ wherein the S1 surface state at \bar{A} , which is responsible for the bonding between the first and the third layer, has more dominant coupling with higher energy phonons according to the temperature-dependent imaginary part of self-energy. A previous theoretical study³² on the electron-phonon coupling of the surface state in Be(0001), of which surface layer largely thermally expands with increasing temperature,²⁷ shows, however, that the low-energy Rayleigh phonon mode took an important role. It is very likely that an additional electron-phonon coupling term should be included in Eq. (1) for the surface free energy $F(d_{12}, T)$ in order to properly explain the thermal dynamic behavior of surface lattice.

IV. CONCLUSIONS

In conclusion, by means of first-principles calculations, we have successfully correlated the surface lattice behavior of Be(10 $\bar{1}$ 0) to the structures and behaviors of three major surface related states, S1, S2, and SR, which disperse in the

large projected bulk band gap between \bar{A} and $\bar{\Gamma}$. Hybridization of S2 and SR constitutes the covalentlike bonding between the atoms of adjacent layers near the surface region, which in turn contributes to the large inward relaxation. A previous study on the surface core level of Be(10 $\bar{1}$ 0) reveals that the largest surface core level shift comes from the second layer instead of the first layer.³³ Most recently, Glans *et al.*³⁴ even assigned the largest shift to layer 2, the second largest shift to layers 3 and 4, and the smallest shift to layer 1. Figures 2(a) and 2(c) clearly show that most of the hybridized charges of S2 and SR are distributed between the first and the second layer, and the rest are in the region between the second and the fourth layer. The covalentlike bonding constituted by the hybridized charges certainly makes it unlikely to screen core level electrons in this region. In other words, large surface core level shifts directly reflect strong covalent bonding in the hybridized region. The S1 surface state, due to its high corrugation on top of the surface, undergoes the Smoluchowski effect, which contributes to the

inward surface relaxation, but as for thermal contraction, the gradual movement of the charge density from the top of the surface to the region between the first and third layers with increasing temperature may indicate a preferred coupling of the S1 surface state with a higher energy phonon related to the bonding between the first and the third layer. Further theoretical work is needed to explain the details of this behavior.

ACKNOWLEDGMENTS

This research was supported by U.S. DOE Contract No. DE-FG02-98ER45712, NSF Contract Nos. DMR-0105232 and DMR-0504654, and National Science Council of Taiwan Grant No. NSC 95-2120-M-007-061 and NSC 95-2112-M-007-062-MY3. The experiment was performed at the ALS of LBNL, which is operated by the DOE's Office of BES, Division of Materials Sciences and Engineering (DE-AC03-76SF00098).

*sjtang@phys.nthu.edu.tw

†jeng@phys.sinica.edu.tw

¹R. Smoluchowski, *Phys. Rev.* **60**, 661 (1941).

²M. W. Finnis and V. Heine, *J. Phys. F: Met. Phys.* **4**, L37 (1974).

³U. Landman, R. N. Hill, and M. Mostoller, *Phys. Rev. B* **21**, 448 (1980), R. N. Barnett, U. Landman, and C. L. Cleveland, *Phys. Rev. B* **28**, 1685 (1983).

⁴P. J. Feibelman, *Phys. Rev. B* **46**, 2532 (1992).

⁵J.-H. Cho, Ismail, Z. Zhang, and E. W. Plummer, *Phys. Rev. B* **59**, 1677 (1999).

⁶*Electronic Surface and Interface States on Metallic Systems*, edited by E. Bertel and M. Donath (World Scientific, Singapore, 1995), p. 15.

⁷Vasile Chis and Bo Hellsing, *Phys. Rev. Lett.* **93**, 226103 (2004).

⁸M. J. G. Lee, M. Gensch, A. I. Shkrebtii, Th. Herrmann, W. Richter, N. Esser, and Ph. Hofmann, *Phys. Rev. B* **72**, 085408 (2005).

⁹L. I. Johansson, H. I. P. Johansson, J. N. Andersen, E. Lundgren, and R. Nyholm, *Phys. Rev. Lett.* **71**, 2453 (1993).

¹⁰P. T. Sprunger, L. Peteren, E. W. Plummer, E. Laegsaard, and F. Besenbacher, *Science* **275**, 1764 (1997).

¹¹M. Hengsberger, D. Purdie, P. Segovia, M. Garnier, and Y. Baer, *Phys. Rev. Lett.* **83**, 592 (1999); M. Hengsberger, R. Fresard, D. Purdie, P. Segovia, and Y. Baer, *Phys. Rev. B* **60**, 10796 (1999).

¹²T. Balasubramanian, E. Jensen, X. L. Wu, and S. L. Hulbert, *Phys. Rev. B* **57**, R6866 (1998).

¹³S. Lashell, E. Jensen, and T. Balasubramanian, *Phys. Rev. B* **61**, 2371 (2000).

¹⁴H. I. P. Johansson, L. I. Johansson, E. Lundgren, J. N. Andersen, and R. Nyholm, *Phys. Rev. B* **49**, 17460 (1994).

¹⁵Ph. Hofmann, B. G. Briner, M. Doering, H.-P. Rust, E. W. Plummer, and A. M. Bradshaw, *Phys. Rev. Lett.* **79**, 265 (1997).

¹⁶Ph. Hofmann, K. Pohl, R. Stumpf, and E. W. Plummer, *Phys. Rev. B* **53**, 13715 (1996).

¹⁷Jun-Hyung Cho, Kwang S. Kim, Sung-Hoon Lee, Myung-Ho Kang, and Zhenyu Zhang, *Phys. Rev. B* **61**, 9975 (2000).

¹⁸Ismail, Ph. Hofmann, A. P. Baddorf, and E. W. Plummer, *Phys.*

Rev. B **66**, 245414 (2002).

¹⁹M. Lazzeri and Stefano de Gironcoli, *Phys. Rev. B* **65**, 245402 (2002).

²⁰S.-J. Tang, Ismail, P. T. Sprunger, and E. W. Plummer, *Phys. Rev. B* **65**, 235428 (2002).

²¹V. M. Silkin and E. V. Chulkov, *Phys. Solid State* **37**, 1540 (1995).

²²Ph. Hofmann, R. Stumpf, V. M. Silkin, E. V. Chulkov, and E. W. Plummer, *Surf. Sci.* **355**, L278 (1996).

²³T. Balasubramanian, L. I. Johansson, P.-A. Glans, C. Virojanadara, V. M. Silkin, E. V. Chulkov, and P. M. Echenique, *Phys. Rev. B* **64**, 205401 (2001).

²⁴P. E. Blochl, *Phys. Rev. B* **50**, 17953 (1994); G. Kresse and D. Joubert, *ibid.* **59**, 1758 (1999).

²⁵G. Kresse and J. Hafner, *Phys. Rev. B* **48**, 13115 (1993); G. Kresse and J. Furthmuller, *Comput. Mater. Sci.* **6**, 15 (1996); *Phys. Rev. B* **54**, 11169 (1996).

²⁶P. J. Feibelman, *Phys. Rev. B* **53**, 13740 (1996).

²⁷K. Pohl, J.-H. Cho, K. Terakura, M. Scheffler, and E. W. Plummer, *Phys. Rev. Lett.* **80**, 2853 (1998).

²⁸F. Theilmann, R. Matzdorf, G. Meister, and A. Goldmann, *Phys. Rev. B* **56**, 3632 (1997).

²⁹R. Paniago, R. Matzdorf, G. Meister, and A. Goldmann, *Surf. Sci.* **336**, L113 (1995).

³⁰We have integrated the charge densities of occupied S1 bands at k points along the two major symmetry directions from \bar{A} to $\bar{\Gamma}$ and from \bar{A} to \bar{L} respectively, and the resulting z profile of charge density distribution is consistent with that at \bar{A} .

³¹S. Narasimhan, *Phys. Rev. B* **64**, 125409 (2001).

³²A. Eiguren, S. de Gironcoli, E. V. Chulkov, P. M. Echenique, and E. Tosatti, *Phys. Rev. Lett.* **91**, 166803 (2003).

³³S. Lizzit, K. Pohl, A. Baraldi, G. Comelli, V. Fritzsche, E. W. Plummer, R. Stumpf, and Ph. Hofmann, *Phys. Rev. Lett.* **81**, 3271 (1998).

³⁴P.-A. Glans, L. I. Johansson, T. Balasubramanian, and R. J. Blake, *Phys. Rev. B* **70**, 033408 (2004).